

Observation and characterization of a non-Abelian gauge field's Wilczek-Zee phase by the Wilson loop

Seiji Sugawa,^{1,2,3,*} Francisco Salces-Carcoba,¹ Yuchen Yue,¹ Andika Putra,^{1,†} and I. B. Spielman¹

¹*Joint Quantum Institute, National Institute of Standards and Technology and the University of Maryland, 100 Bureau Dr., National Institute of Standards and Technology, Gaithersburg, Maryland 20899-8424 USA*

²*PRESTO, Japan Science and Technology, Tokyo 102-0076 Japan*

³*Graduate School of Science, Kyoto University, Kyoto 606-8502 Japan*

(Dated: July 8, 2022)

Quantum states can acquire a phase called the Berry phase after adiabatically traversing a closed loop in parameter space. This phase is geometric – dependent on the path – not the rate of motion. Wilczek and Zee extended this concept to include non-Abelian phases that can be characterized the Wilson loop, a gauge independent quantity. Here we quantum-engineer a non-Abelian SU(2) gauge field for an atomic Bose-Einstein Condensate (BEC), in a 5-dimensional “synthetic” parameter space derived from internal atomic degrees of freedom. By slowly encircling a topological monopole, we observed the adiabatic Wilczek-Zee phase that we characterize in terms of the Wilson loop.

The seemingly abstract geometry of a quantum system's eigenstates now finds application in fields ranging from condensed-matter and high-energy physics to quantum information science. For example, the topological classification of crystalline materials derives from such geometric quantities (Berry curvature) integrated over a closed manifold such as a crystal's Brillouin zone [1]. The Berry phase – a geometric phase acquired as a single (non-degenerate) quantum state follows a closed loop (i.e. cyclic motion) in any parameter space [2] – provides a prime observable associated with this geometry. It has been measured in a variety of physical systems, and the concept, including extensions to non-adiabatic and non-cyclic motion, as well as to mixed states appears throughout physics and chemistry [3–7].

In 1984, Wilczek and Zee [8] extended Berry's idea to include non-Abelian geometric phases by considering cyclic evolution of states within a degenerate manifold. Following the initial nuclear magnetic resonance experiments [9, 10], the non-Abelian geometric phase inspired holonomic quantum computation that utilizes the operator-valued Wilczek-Zee (W.-Z.) phase to affect noise-resistant geometric quantum gates [11]. Holonomic quantum gates have been demonstrated both in the adiabatic limit [12] and in the diabatic limit [13–15]. However, despite the universality of Wilczek and Zee's concept, there were only a few observations [12, 16, 17] of adiabatic W.-Z. phase in any physical system, and even with many proposals [18–24] this phase has not been observed for ultracold atoms.

In this Article, we observed and characterized the W.-Z. phase in an atomic Bose-Einstein condensate. This phase was acquired from near-adiabatic evolution of the quantum state within a degenerate manifold, built in the synthetic dimensional parameter space derived from rf and microwave coupled atomic hyperfine states.

Time evolution in the degenerate manifold was governed by a non-Abelian SU(2) gauge field. Our scheme utilized a degenerate subspace (DS) of the system's Hilbert space, that was insensitive to noise, including environmental magnetic field fluctuation. We confirmed the non-Abelian operator character of the W.-Z. phase factor using quantum process tomography, and characterized it in terms of the gauge-independent Wilson loop. The Wilson loop is not uniquely defined: in the condensed-matter literature the non-Abelian holonomy \hat{U} is used synonymously with the Wilson loop, whereas in other contexts such as high-energy physics, $\text{tr}(\hat{U})$ is associated with the Wilson loop. Both conventions are present in the quantum-gas literature, and we have adopted the latter definition. We further show that even for the same path, these geometric properties depend on the direction the path is followed.

Berry showed that, for a single non-degenerate energy state, the Abelian Berry connection (gauge field) is gauge dependent [2], but both the Berry phase and Berry curvatures are gauge independent. These quantities are invariant under gauge transformation by unitary operation $U = e^{i\Phi(\mathbf{q})}$ that depends on position-dependent phase $\Phi(\mathbf{q})$ in the parameter space. In a degenerate manifold, where the gauge field is generally non-Abelian, the non-Abelian extensions of Berry's phase and curvatures are no longer gauge invariant. The Wilson loop, defined as trace of the W.-Z. phase factor (non-Abelian holonomy) is an important non-local gauge-independent geometric quantity. It was originally considered for the problem of quark-confinement [25, 26] and has been often used in formulating gauge theories. In topological quantum computation, Wilson loop describes braiding evolution of non-Abelian anyons [27, 28]. Moreover, in crystalline systems – including both conventional materials and synthetic quantum matter – the eigenspectrum of the Wilson loop can characterize the topology of the Bloch bands [29, 30]. Ultracold atoms subject to non-Abelian gauge potentials enable well-controlled experiments exploring a range of

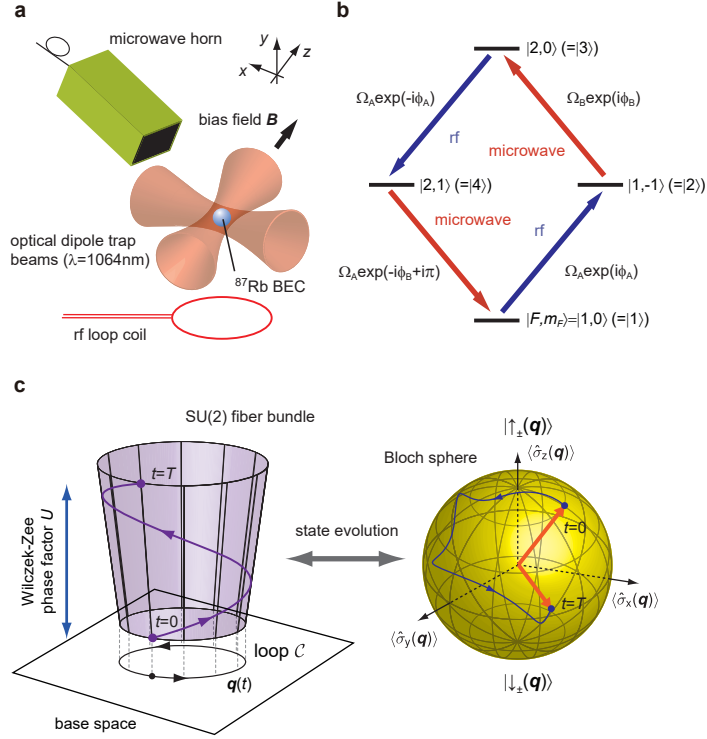


FIG. 1. **Wilczek-Zee phase measurement.** **a** Schematic. A ^{87}Rb Bose-Einstein condensate (BEC) subject to uniform bias magnetic field was illuminated with rf and microwave fields which coupled its hyperfine ground states. **b** Cyclically coupled four-level system realized with hyperfine ground states of ^{87}Rb . **c** Fiber-bundle description of the W.-Z. phase in the degenerate subspace. The two-fold degenerate state space \mathcal{S}_2 has a $\text{SU}(2)$ gauge degree of freedom that is encoded in the fiber. When the quantum state is adiabatically changed along a path \mathcal{C} in the base space, the parallel transport condition sets vertical lift along the fiber. The final state $|\Psi_f\rangle$ after closing the path is different from the initial state $|\Psi_i\rangle$ by a factor of the holonomy U_C due to the acquisition of W.-Z. phase. This state evolution in our degenerate subspace can be represented by the trajectory of the Bloch vector.

geometric and topological phenomena [31–34] for application in quantum simulation. In this present work we use this control to present the first measurement of the Wilson loop for adiabatic motion within a degenerate manifold.

In the framework of differential geometry [35], adiabatic motion is described in terms of fiber bundles, where the fibers represent the gauge degree of freedom. As the state adiabatically evolves, the parallel transport condition sets the choice of basis state, which leads to vertical lift along the fiber (Fig. 1c). After tracing out a closed loop \mathcal{C} in space, the state will have evolved according to the unitary transformation

$$\hat{U}_C = \mathcal{P} \exp \left(i \int_C \hat{\mathcal{A}}_q \cdot dq \right), \quad (1)$$

which is the W.-Z. geometric phase factor, i.e., the non-Abelian holonomy. Here \mathcal{P} indicates that the exponential should be evaluated in a path-ordered manner and $\hat{\mathcal{A}}_q$ is the non-Abelian gauge field (non-Abelian Berry connection). The Wilson loop $W = \text{tr}(\hat{U})$ is manifestly gauge independent, and for a single non-degenerate en-

ergy level, it reduces to Berry’s phase factor.

Our experiments began with an optically trapped ^{87}Rb BEC, from which we engineered a non-Abelian $\text{SU}(2)$ gauge field by cyclically coupling four hyperfine ground states [34]. The four spin states – $|F, m_F\rangle = |1, 0\rangle (\equiv |1\rangle)$, $|1, -1\rangle (\equiv |2\rangle)$, $|2, 1\rangle (\equiv |3\rangle)$ and $|2, 0\rangle (\equiv |4\rangle)$ – were coupled with rf and microwave fields parameterized by two Rabi frequencies Ω_A and Ω_B with phases ϕ_A and ϕ_B [See Fig. 1b]. The system then evolved according to the Hamiltonian

$$\hat{H} = -\frac{\hbar}{2} \sum_{i=1}^5 q_i \hat{\Gamma}_i, \quad (2)$$

expressed in terms of the five Dirac gamma matrices $\hat{\Gamma}_i$, where the vector $\mathbf{q} = (q_1, q_2, q_3, q_4, q_5)$ defines coordinates in a five-dimensional parameter space and \hbar is the reduced Planck constant. Here the five-dimensional control vector \mathbf{q} is determined by laboratory parameters $q_1 = -\Omega_B \cos \phi_B$, $q_2 = -\Omega_A \cos \phi_A$, $q_3 = -\Omega_A \sin \phi_A$, $q_4 = 0$, and $q_5 = -\Omega_B \sin \phi_B$.

We focused on the near-adiabatic control of the rf phase ϕ_A for a range of coupling ratios ($\Omega_B/\Omega_A = \tan \theta_2$)

at fixed microwave phase $\phi_B = 0$. The energy spectrum always consisted of a pair of two-fold degenerate energy manifolds with eigenstates $\{|\uparrow_-(\mathbf{q})\rangle, |\downarrow_-(\mathbf{q})\rangle\}$ for the ground state manifold and $\{|\uparrow_+(\mathbf{q})\rangle, |\downarrow_+(\mathbf{q})\rangle\}$ for the excited state manifold. The energy gap was measured by inducing coherent Rabi-like oscillations between the eigenstates. Throughout this manuscript, the gap ($\Delta E(\mathbf{q}) = \hbar\sqrt{\Omega_A^2 + \Omega_B^2}$) is $h \times 2.0$ kHz. Due to the two-fold DS, the underlying gauge field $\hat{\mathcal{A}}$ is non-Abelian and has SU(2) symmetry. When \mathbf{q} is adiabatically changed along a closed path, the quantum state evolves within the subspace and acquires W.-Z. phases. This geometric process can be viewed as a hypothetical particle moving acquired around the non-Abelian Yang monopole, which can be regarded as a source of the SU(2) gauge field [34, 36].

The consequence of the acquired W.-Z. phase can be experimentally captured by explicitly following an initial state as it evolves within the DS as a result of adiabatically moving \mathbf{q} in parameter space. To this end, we first prepared one of the eigenstates ($|\uparrow_-(\mathbf{q}_0)\rangle = 1/\sqrt{2}|1\rangle - 1/2|2\rangle + 1/2|4\rangle$) at $\mathbf{q}_0 = (-\Omega_B, -\Omega_A, 0, 0, 0)$ in the ground state manifold. After the state preparation, we linearly ramped the rf phase ($\phi_A(t) = 2\pi t/T$, where $T = 2$ ms), tracing out the closed loop \mathcal{C}_+ shown in the left panel of Fig. 2a. We perform state tomography within the DS to compare the final state with the initial state (See Methods).

The state within the DS is captured by the Bloch vector in a Bloch sphere. The states before and after the control sequence are shown in the right panel of Fig. 2a. It can be clearly seen that the Bloch vector is rotated even though the final control parameters are the same as the initial ones, manifesting the matrix nature of the W.-Z. phase factor's representation. This is striking in contrast with the Abelian Berry phase, which would leave the orientation on the Bloch sphere unchanged.

The consequence of the geometric phase acquisition also depends on the direction of the ramp. For the Abelian case, a reversed ramp along the same loop results in the same phase with its sign flipped. However, for the non-Abelian case, this relation does not hold. Figure 2b shows the experimental result for reversed phase ramp along the same path, where the final state is rotated in a different way. We denote the motion along the same path in different directions by \mathcal{C}_+ for the phase-increasing ramp and \mathcal{C}_- for the reversed ramp. In the following sections, we will see that the seemingly unrelated results between the opposite ramps can be captured by process tomography and Wilson loop measurement.

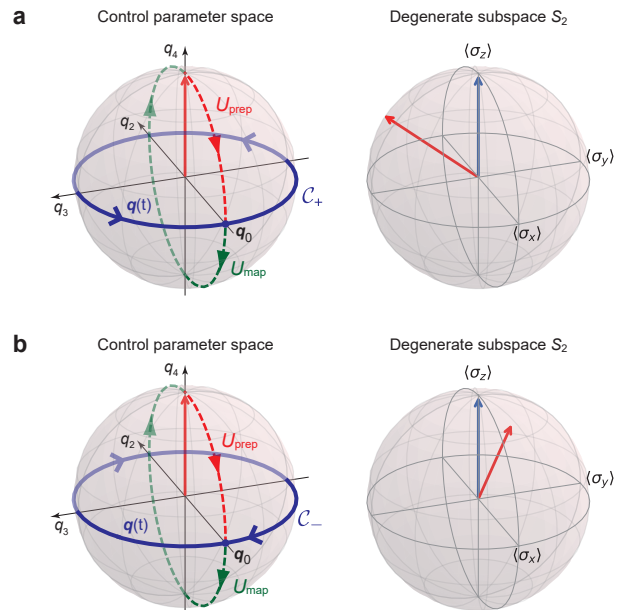


FIG. 2. **Acquisition of W.-Z. phase within the degenerate subspace.** **a** (Left panel) Schematic of the control sequence for observing W.-Z phase for the path \mathcal{C}_+ . A microwave and rf pulse rotate the control field from $\mathbf{q}_N \parallel (0, 0, 0, 1, 0)$ to \mathbf{q}_0 to prepare the eigenstate at \mathbf{q}_0 (red curve). The control vector \mathbf{q} traces out a closed loop \mathcal{C} by linearly ramping the rf phase for time duration T , such that $\mathbf{q}(t) = (-\Omega_B, -\Omega_A \cos(2\pi t/T), -\Omega_A \sin(2\pi t/T), 0, 0)$ (blue curve). The state is mapped to \mathbf{q}_N for state read-out by applying another pulse (green curve). The preparation and mapping pulse give one-to-one correspondence between the state within the DS at \mathbf{q}_0 and \mathbf{q}_N . For illustrative purpose, only three dimensions in the control field space are shown. (Right panel) Bloch vector within the DS measured after the control sequence for the path \mathcal{C}_+ is compared with the initial one $\langle \hat{\sigma} \rangle = (0, 0, 1)$ (blue arrows). The final Bloch vector was $\langle \hat{\sigma} \rangle = (-0.62(3), -0.70(5), 0.47(2))$ (red arrows). **b** (Left panel) The control sequence for observing W.-Z phase for the path \mathcal{C}_- , which takes the opposite ramp direction for tracing out the loop \mathcal{C} . (Right panel) The initial $\langle \hat{\sigma} \rangle = (0, 0, 1)$ (blue arrow) and the final Bloch vectors $\langle \hat{\sigma} \rangle = (-0.68(1), 0.59(5), 0.40(5))$ (red arrows) after tracing out a loop are shown. The laboratory parameters are $\Omega_A = \Omega_B = h \times 1.4$ kHz.

To fully characterize the process accompanying the W.-Z. phase acquisition, we perform quantum process tomography [37, 38] within the ground state DS. An arbitrary transformation (operation) on a quantum system with initial density operator $\hat{\rho}_{\text{ini}}$ can be described by the action of Kraus operators \hat{K}_k : $\hat{\rho}_{\text{fin}} = \sum_k \hat{K}_k \hat{\rho}_{\text{ini}} \hat{K}_k^\dagger$. The Kraus operators \hat{K}_k completely describe the whole process, and can be expanded by a basis for operators $\{\hat{E}_i\}$ as $\hat{K}_k = \sum_i c_{ki} \hat{E}_i$, where $c_{ki} \in \mathbb{C}$ is the coefficient. Thus, the density operator encoding the state within the DS

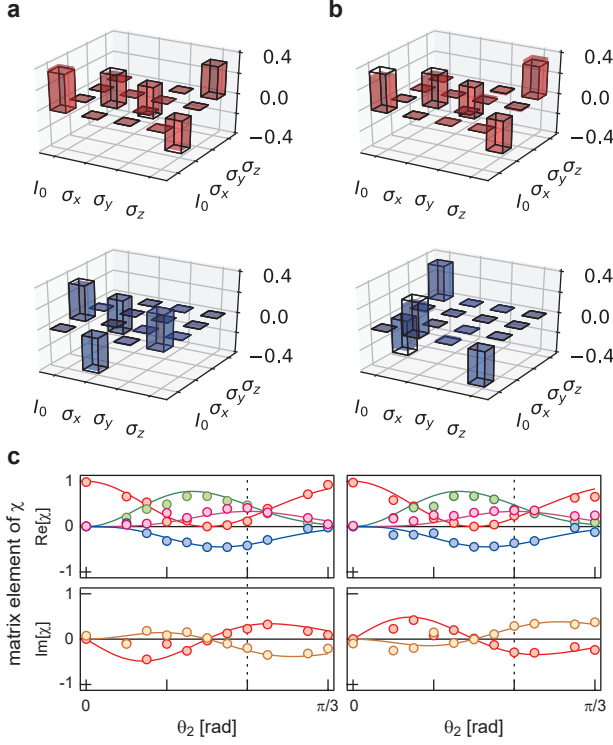


FIG. 3. **Process tomography of W.-Z. phase.** Reconstructed process matrices χ_{ij} of the non-Abelian holonomy \hat{U}_C for (a) forward and (b) reversed ramps at $\theta_2 = \pi/4$. Theoretical results are shown in solid black frames. The fidelity of the geometric process reached $\mathcal{F}_{C_+} = 0.98$ and $\mathcal{F}_{C_-} = 0.96$ for forward and reversed ramp, respectively. **c** Process matrix components (χ_{ij}) for forward (left panels) and reverse (right panels) ramps for different W.-Z. phase realizations. The top panel shows the real parts [χ_{00} (red), χ_{xx} (green), χ_{zz} (purple), χ_{xz} (blue)] and the bottom panels shows the imaginary parts [χ_{0x} (red), χ_{0z} (orange)]. The characteristic of the non-Abelian holonomy, $\hat{U}_{C_-} = \hat{U}_{C_+}^\dagger$, can be clearly seen in the real and imaginary parts of χ_{ij} . The solid lines are the theory.

transforms as $\hat{\rho}_{\text{fin}} = \sum_{i,j} \hat{E}_i \hat{\rho}_{\text{ini}} \hat{E}_j^\dagger \chi_{ij}$, with weights given by the process matrix $\chi_{ij} = \sum_k c_{ki} c_{kj}^*$. In the following, we take $\{\hat{E}_i\} = \{\hat{I}_0, \hat{\sigma}_x, \hat{\sigma}_y, \hat{\sigma}_z\}$ as the basis. The process matrix χ completely and uniquely represents our experimental W.-Z. phase acquisition process. In theory, its element χ_{ij} is analytically obtained from the non-Abelian W.-Z. phase factor \hat{U} as $\chi_{ij} = \text{tr}(\hat{U} \hat{E}_i) \text{tr}(\hat{U} \hat{E}_j)^* / 4$.

We experimentally obtain the process matrix χ by repeating the measurement illustrated in Fig. 2 for four-independent initial states ($|A\rangle = |\uparrow_-(\mathbf{q}_0)\rangle$, $|B\rangle = |\downarrow_-(\mathbf{q}_0)\rangle$, $|C\rangle = (|A\rangle + |B\rangle)\sqrt{2}$, $|D\rangle = (|A\rangle + i|B\rangle)\sqrt{2}$) and applying maximum likelihood estimation to obtain physical χ , which is positive semi-definite and Hermite (See Methods).

Figure 3a, b illustrate the reconstructed process matrices of the non-Abelian W.-Z. phase obtained for the forward and the reverse ramps at $\theta_2 = \pi/4$. The two re-

sults for opposite ramps along the same path show that the real part of χ takes almost the same values, whereas the imaginary parts of χ have the opposite sign. This trend can be explained from the definition of the W.-Z. phase (Eq. (1)) satisfying the relation $\hat{U}_{C_+} = \hat{U}_{C_-}^\dagger$ and thus $\chi_{ij}(C_+) = \chi_{ij}^*(C_-)$ for the process matrices of the non-Abelian W.-Z. phase. The above behavior of the process matrix elements holds for different coupling ratios (i.e. θ_2) as shown in Fig. 3c, where different kinds of non-Abelian W.-Z. phases are realized. The result, which is in stark contrast to the Abelian Berry phase, is in excellent agreement with the generalized relation for holonomy.

The process matrix allows us to evaluate the fidelity of our holonomic control within the DS. Using the analytical expression for the non-Abelian holonomy \hat{U}_C , the fidelity of the process shown in Fig. 3 a, b reached as high as $\mathcal{F}_{C_+} = 0.98$ for forward ramp and $\mathcal{F}_{C_-} = 0.96$ for reverse ramp even for finite ramp time. Here the fidelity is defined as $\mathcal{F} = \text{tr}(\chi_{\text{th}} \chi)$, where χ_{th} is theoretical process matrix assuming adiabaticity. The high fidelity, which is realized by focusing on the DS, enabled us to characterize the W.-Z. phase with high accuracy. It has been argued that the non-adiabatic effect does not contribute to the state evolution in the DS up to first order, even though the state deflects from the adiabatic limit [34, 39].

All the above measurements depend on the choice of the basis, i.e. gauge, whereas the Wilson loop does not. From the process matrix components measured in Fig. 3, the absolute value of the Wilson loop is $|W_C| = 2\sqrt{\chi_{11}}$. Figure 4 shows $|W_C|$ for forward (C_+) and reverse ramp (C_-) as the path \mathcal{C} is varied by changing coupling ratio (Ω_A/Ω_B). The theoretical relation for the opposite ramp on the same path ($|W_{C_+}| = |W_{C_-}|$) can be clearly observed in experimental data, which also shows good agreement with the analytical curve for adiabatic control. At $\theta_2 = 0$, the geometric phase is simply $\hat{U}_C = -\hat{I}_0$ and $W_{C_\pm} = -2$ resulting from simultaneous control of two-level systems, acquiring the Berry phase of $\pm\pi$. The experimental result shows the maximum change of the possible $|W_C|$ (i.e from 0 to 2), manifesting the non-Abelian nature of the geometric property. Since the system is time-reversal invariant, the global phase factor should be $\pm n\pi$ (n is an integer) and the Wilson loop's value is real. The Wilson loop is robust against some perturbation. Although circular paths is chosen here, the Wilson loop is unchanged as long as the path in the polar coordinate (Ω, ϕ_A) encloses the topological Yang monopole.

The eigenvalues of the W.-Z. phase factor can be also evaluated from our measurement. Since holonomy is a unitary operator, the magnitude of its eigenvalues is always one. By defining λ_1 and λ_2 as the argument of the complex eigenvalues, the relation $W_C =$

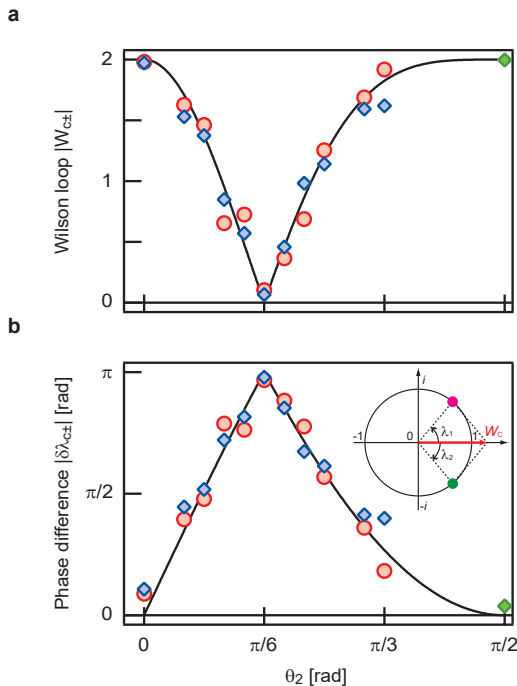


FIG. 4. **Measurement of Wilson loop and eigenvalues of W.-Z phase factor.**

a Absolute values of the Wilson loop along the closed path \mathcal{C} are measured for forward (W_{C_+} , blue diamonds) and reverse ramps (W_{C_-} , red circles). At $\theta_2 = \pi/2$, the circular paths converge to a point, where we also measure with $T=0$ (a green diamond). Theory curves for $|W_{C_{\pm}}|$ (solid line) are also shown. **b** The phase difference of the eigenvalues of W.-Z phase factor $|\delta\lambda_{C_{\pm}}|$ obtained from the Wilson loop measurement in **a**. The phases for forward ($|\delta\lambda_{C_+}|$, blue diamonds) and reverse ramps ($|\delta\lambda_{C_-}|$, red circles) are shown with theory curves for $|\delta\lambda_{C_{\pm}}|$ (solid line). The reference point at $\pi/2$ is also shown (a green diamond). The eigenvalues satisfy $W_C = \exp(i\lambda_1) + \exp(i\lambda_2)$ as graphically illustrated in the inset. In the complex plane, the eigenvalues appear on the unit circle (pink and green points), and the sum gives the Wilson loop (red arrow). As our system has time-reversal symmetry, $\lambda_1 = -\lambda_2$ is met. The pair of phases are determined up to phase uncertainty in $n\pi$, where n is an integer. At $\theta_2 = \pi/6$, the phases are $\lambda_1 = -\lambda_2 = \pi/2 + n\pi$, where the pair of eigenvalues are determined to be $\{-i, i\}$.

$\exp(i\lambda_1) + \exp(i\lambda_2)$ is met. Thus, the Wilson loop is a measure of the phase difference of these eigenvalues, which is also gauge-independent. We extract the phase difference $\delta\lambda = |\lambda_1 - \lambda_2| \in [0, \pi]$ from the Wilson loop measurement, showing good agreement with the theory (see Fig. 4 **b**). By noting that our system is time-reversal invariant (TRI), Wilson loop is real and $\lambda_1 = -\lambda_2$ is satisfied. Thus, eigenvalues of W.-Z. phase factor can be measured from Wilson loop for TRI system.

Finally, we show measurement on the Wilson line on open paths by observing non-cyclic W.-Z. phases. The non-cyclic W.-Z. phases is defined by simply re-

placing the closed path for the integral in Eq. (1) with an open path \mathcal{C} . The Wilson line, defined as the trace of the non-cyclic W.-Z. phase factor, is not gauge-independent, and thus it depends on the choice of the basis at both ends of the path. The experimental procedure is the same as the Wilson loop measurement, except the rf phase ramp is halted at variable phase $\phi_A = \phi$ ranging from 0 to 2π . After preparing the eigenstates at \mathbf{q}_0 , we ramp the control vector as $\mathbf{q}(t) = (-\Omega_B, -\Omega_A \cos(2\pi t/T), -\Omega_A \sin(2\pi t/T), 0, 0)$ for $t = [0, \phi T/2\pi]$ until the control vector reaches $\mathbf{q}_f = (-\Omega_B, -\Omega_A \cos \phi, -\Omega_A \sin \phi, 0, 0)$. The final state within the DS at \mathbf{q}_f is always mapped to the DS at $\mathbf{q} = \mathbf{q}_0$ for the state tomography. By performing the process tomography for the four-independent eigenstates, the process matrix of the non-cyclic non-Abelian geometric phase is reconstructed in the same manner as in Fig. 3 for each phase. Figure 5 shows the obtained Wilson lines from the reconstructed process matrices for a choice of the basis states based on our experimental procedure (See Method). The Wilson line is trivially $W_C = 2$ at $\phi = 0$ and becomes gauge-independent at $\phi = 2\pi$ where the trajectory is closed.

The whole unitary process including the state preparation and the state mapping processes can be viewed as a local gauge transformation of the W.-Z phase: $\hat{U}_C \rightarrow V(\mathbf{q}_f)\hat{U}_C V^\dagger(\mathbf{q}_0) = -\hat{U}_{\text{map}}(\phi)\hat{U}_C\hat{U}_{\text{prep}}$, where $V(\mathbf{q})$ is a position-dependent unitary operator, and \hat{U}_{prep} (\hat{U}_{map}) is a unitary operator that represents the pulse that maps the state within the DS at $\mathbf{q}_N(\mathbf{q}_f)$ to the state within the DS at \mathbf{q}_0 . This clearly illustrates that the Wilson line is gauge-independent only when $\mathbf{q}_f = \mathbf{q}_0$, where it becomes equivalent to the Wilson loop.

In conclusion, we observed cyclic and non-cyclic W.-Z phases acquired from a non-Abelian gauge field, the source of which is a Yang monopole located at $\mathbf{q} = \mathbf{0}$. Due to the high SO(5) symmetry around the monopole in five-dimensional space, the Wilson loop is robust against some deformation of the path. By varying the closed path, we explored the whole range of the Wilson loop, showing essentially the full set of the SU(2) holonomic control. Additional Ramsey interference measurements will allow for determination of the sign of the Wilson loop. Moreover, the combination of rf and microwave phase control will enable us to verify the non-commuting nature of W.-Z. phases. The rf and microwave coupling used here can be replaced with a set of Raman lasers to realize non-Abelian SU(2) gauge field, where various exotic many-body phenomena are accessible using ultracold atoms [40]. Our coupling and measurement scheme can be broadly extended to other quantum systems including trapped ions, superconducting qubits, NV centers and other solid-state spins, where equivalent coupling is possible. Therefore, our present work may pave the way

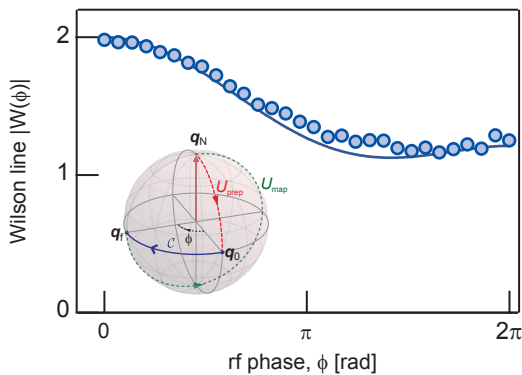


FIG. 5. **Measurement of Wilson line.** Absolute values of measured Wilson line $|W(\phi)|$ for open paths with variable path length characterized by rf phase range ϕ . Theory curve (solid line) also shown. The inset illustrates the control sequence for Wilson line measurement of a segment from \mathbf{q}_0 to \mathbf{q}_f on a circular loop. After preparing one of the eigenstates at \mathbf{q}_0 , the rf phase ϕ_A is ramped from 0 to ϕ . The red and green curves represent the pulse controls for the state preparation and the state mapping for the read-out. The laboratory parameters are $\Omega_A = \Omega_B = h \times 1.4$ kHz.

for applications in precision measurement (e.g. magnetometry [41]), quantum gate operations, and quantum simulation using adiabatic W.-Z phases.

Acknowledgement

We acknowledge the support for this work provided by the AFOSRs Quantum Matter MURI, NIST and the NSF through the PFC at the JQI. S.S. acknowledges support from JST, PRESTO (JPMJPR1664) and JSPS (fellowship for research aboard). We thank Mingwu Lu and Chris Billington for carefully reading our manuscript.

* Present Address: Institute for Molecular Science, National Institutes of Natural Sciences, Myodaiji, Okazaki 444-8585, Japan & SOKENDAI (The Graduate University for Advanced Studies), Myodaiji, Okazaki 444-8585, Japan

† Present Address: The MathWorks, Inc., 3 Apple Hill Drive, Natick, Massachusetts 01760 USA

- [1] B. A. Bernevig and T. L. Hughes, *Topological insulators and topological superconductors* (Princeton university press, 2013).
- [2] M. V. Berry, Proc. R. Soc. Lond. A **392**, 45 (1984).
- [3] J. Zak, Phys. Rev. Lett. **62**, 2747 (1989).
- [4] Y. Zhang, Y.-W. Tan, H. L. Stormer, and P. Kim, Nature **438**, 201 (2005).
- [5] A. Bohm, A. Mostafazadeh, H. Koizumi, Q. Niu, and J. Zwanziger, *The Geometric Phase in Quantum Systems: Foundations, Mathematical Concepts, and Ap-*

plications in Molecular and Condensed Matter Physics (Springer Science & Business Media, 2013).

- [6] B. K. Kendrick, J. Hazra, and N. Balakrishnan, Nature Communications **6**, 7918 (2015).
- [7] P. J. Leek, J. M. Fink, A. Blais, R. Bianchetti, M. Goppl, J. M. Gambetta, D. I. Schuster, L. Frunzio, R. J. Schoelkopf, and A. Wallraff, Science **318**, 1889 (2007).
- [8] F. Wilczek and A. Zee, Phys. Rev. Lett. **52**, 2111 (1984).
- [9] R. Tycko, Phys. Rev. Lett. **58**, 2281 (1987).
- [10] J. Zwanziger, M. Koenig, and A. Pines, Phys. Rev. A **42**, 3107 (1990).
- [11] L.-M. Duan, J. I. Cirac, and P. Zoller, Science **292**, 1695 (2001).
- [12] K. Toyoda, K. Uchida, A. Noguchi, S. Haze, and S. Urabe, Phys. Rev. A **87**, 052307 (2013).
- [13] A. A. Abdumalikov Jr, J. M. Fink, K. Juliusson, M. Pechal, S. Berger, A. Wallraff, and S. Filipp, Nature **496**, 482 (2013).
- [14] C. Zu, W.-B. Wang, L. He, W.-G. Zhang, C.-Y. Dai, F. Wang, and L.-M. Duan, Nature **514**, 72 (2014).
- [15] S. Arroyo-Camejo, A. Lazariev, S. W. Hell, and G. Balasubramanian, Nature Communications **5**, 4870 (2014).
- [16] F. Leroux, K. Pandey, R. Rehbi, F. Chevy, C. Miniatura, B. Grémaud, and D. Wilkowski, Nature Communications **9**, 3580 (2018).
- [17] Y. Yang, C. Peng, D. Zhu, H. Buljan, J. D. Joannopoulos, B. Zhen, and M. Soljačić, Science **365**, 1021 (2019).
- [18] J. Ruseckas, G. Juzeliūnas, P. Öhberg, and M. Fleischhauer, Phys. Rev. Lett. **95**, 010404 (2005).
- [19] K. Osterloh, M. Baig, L. Santos, P. Zoller, and M. Lewenstein, Phys. Rev. Lett. **95**, 010403 (2005).
- [20] N. Goldman, A. Kubasiak, P. Gaspard, and M. Lewenstein, Phys. Rev. A **79**, 023624 (2009).
- [21] V. Pietilä and M. Möttönen, Phys. Rev. Lett. **102**, 080403 (2009).
- [22] A. Bermudez, N. Goldman, A. Kubasiak, M. Lewenstein, and M. A. Martin-Delgado, New Journal of Physics **12**, 033041 (2010).
- [23] P. Hauke, O. Tieleman, A. Celi, C. Ölschläger, J. Simonet, J. Struck, M. Weinberg, P. Windpassinger, K. Sengstock, M. Lewenstein, *et al.*, Phys. Rev. Lett. **109**, 145301 (2012).
- [24] N. T. Phuc, G. Tatara, Y. Kawaguchi, and M. Ueda, Nature Communications **6**, 8135 (2015).
- [25] K. G. Wilson, Phys. Rev. D **10**, 2445 (1974).
- [26] R. Giles, Phys. Rev. D **24**, 2160 (1981).
- [27] A. Y. Kitaev, Annals of Physics **303**, 2 (2003).
- [28] J. K. Pachos, *Introduction to topological quantum computation* (Cambridge University Press, 2012).
- [29] A. Alexandradinata, X. Dai, and B. A. Bernevig, Phys. Rev. B **89**, 155114 (2014).
- [30] T. Li, L. Duca, M. Reitter, F. Grusdt, E. Demler, M. Endres, M. Schleier-Smith, I. Bloch, and U. Schneider, Science **352**, 1094 (2016).
- [31] H.-I. Lu, M. Schemmer, L. M. Aycok, D. Genkina, S. Sugawa, and I. B. Spielman, Phys. Rev. Lett. **116**, 200402 (2016).
- [32] M. Aidelsburger, M. Lohse, C. Schweizer, M. Atala, J. T. Barreiro, S. Nascimbène, N. R. Cooper, I. Bloch, and N. Goldman, Nature Physics **11**, 162 (2015).
- [33] L. Asteria, D. T. Tran, T. Ozawa, M. Tarnowski, B. S. Rem, N. Fläschner, K. Sengstock, N. Goldman, and C. Weitenberg, Nature Physics **15**, 449 (2019).

- [34] S. Sugawa, F. Salces-Carcoba, A. R. Perry, Y. Yue, and I. Spielman, *Science* **360**, 1429 (2018).
- [35] M. Nakahara, *Geometry, topology and physics* (CRC Press, 2003).
- [36] C. N. Yang, *Journal of Mathematical Physics* **19**, 320 (1978).
- [37] M. Nielsen and I. Chuang, *Quantum computation and quantum information* (Cambridge University Press, 2000).
- [38] D. F. V. James, P. G. Kwiat, W. J. Munro, and A. G. White, *Phys. Rev. A* **64**, 052312 (2001).
- [39] Q. Zhang, *Phys. Rev. A* **93**, 012116 (2016).
- [40] Y.-J. Lin, R. L. Compton, K. Jimenez-Garcia, J. V. Porto, and I. B. Spielman, *Nature* **462**, 628 (2009).
- [41] K. Arai, J. Lee, C. Belthangady, D. R. Glenn, H. Zhang, and R. L. Walsworth, *Nature Communications* **9**, 4996 (2018).

Supplementary information for: Observation and characterization of a non-Abelian gauge field's Wilczek-Zee phase by the Wilson loop

Atom preparation and atom number counting

Bose-Einstein Condensates (BECs) of rubidium-87 of $\approx 1 \times 10^5$ were prepared in a crossed optical dipole trap formed by two horizontal 1064 nm optical trapping beams with the trapping frequencies $(f_x, f_y, f_z) \approx (50, 110, 70)$ Hz, where the y-axis is along the direction of gravity. Initially, the BECs were prepared in the $|1, -1\rangle$ state. Atoms were then transferred to prepare a superposition state of $|1, 0\rangle$ and $|2, 0\rangle$ by rf and microwave pulses, which is the ground state of our Hamiltonian in Eq. (2) at \mathbf{q}_N . The bias magnetic field of 19.8 G pointing along the z-axis was stabilized for long term drift at 2.5 ppm.

We performed an absorption imaging and Stern-Gerlach measurements to resolve the atoms in the hyperfine ground states. After the rf and microwave control was finished, we abruptly turned off the optical dipole trap beams for time-of-flight (TOF). During the TOF, a magnetic field gradient pulse was applied to perform Stern-Gerlach measurement, which separated atoms in $|1, 0\rangle$ and $|2, 0\rangle$ from those in $|1, 1\rangle$ and $|2, -1\rangle$ in space. We imaged the atoms in $F = 2$ manifold by illuminating a probe pulse resonant to $5S_{1/2}, F = 2 \rightarrow 5P_{3/2}, F = 3$ transition after TOF of 23.2 ms. A short repump laser pulse resonant with the $5S_{1/2}, F = 1 \rightarrow 5P_{3/2}, F = 2$ transition was applied before the probe pulse in order to image atoms in $F = 1$ and $F = 2$ manifolds. When we focused on the state in ground DS, we apply a π -pulse resonant with the microwave transition $|1, 0\rangle \leftrightarrow |2, 1\rangle$ to swap the population between the two states right before the TOF and only measure atoms in the $F = 2$ manifold. This allowed us to measure the relative population $(N_\uparrow - N_\downarrow)/(N_\uparrow + N_\downarrow)$ with a single shot image. Here $N_\uparrow(N_\downarrow)$ is the atom number in $|\uparrow\rangle = |1, 0\rangle(|\downarrow\rangle = |2, 0\rangle)$ state before the microwave π -pulse was applied.

The Dirac matrices

As the representation of the Dirac matrices, we take $\hat{\Gamma}_1 = \hat{\sigma}_2 \otimes \hat{\sigma}_2$, $\hat{\Gamma}_2 = \hat{I}_0 \otimes \hat{\sigma}_1$, $\hat{\Gamma}_3 = \hat{\sigma}_3 \otimes \hat{\sigma}_2$, $\hat{\Gamma}_4 = \hat{I}_0 \otimes \hat{\sigma}_3$ and $\hat{\Gamma}_5 = \hat{\sigma}_1 \otimes \hat{\sigma}_2$. Here $\hat{\sigma}_i$, ($i = x, y, z$) are the Pauli operators, \hat{I}_0 is the identity operator, and \otimes is the Kronecker product. Each Dirac matrix has eigenvalues of ± 1 , each of which is two-fold degenerate.

Pulse control for state preparation and state mapping

The unitary operator corresponding to the rf and microwave pulse used for the state preparation and the state mapping is governed by the following time-independent Hamiltonian that describes the cyclic coupling with $\pi/2$ different choice of the rf and microwave phases.

$$\hat{H}_{\text{map}}(\mathbf{q}) = -\frac{\hbar}{2}(q_1\hat{\gamma}_1 + q_2\hat{\gamma}_2 + q_3\hat{\gamma}_3 + q_5\hat{\gamma}_4), \quad (\text{S1})$$

Here $\hat{\gamma}_1 = \hat{\sigma}_2 \otimes \hat{\sigma}_1$, $\hat{\gamma}_2 = -\hat{I}_0 \otimes \hat{\sigma}_2$, $\hat{\gamma}_3 = -\hat{\sigma}_3 \otimes \hat{\sigma}_1$, $\hat{\gamma}_4 = \hat{\sigma}_1 \otimes \hat{\sigma}_1$. The unitary evolution during the pulsing is then

$$\hat{U}_{\text{trans}}(t, \mathbf{q}) = \exp(-i\hat{H}_{\text{map}}(\mathbf{q})t), \quad (\text{S2})$$

where t is the pulse duration, and the state oscillates at a period determined by the energy gap (ΔE) . For $t_{\text{prep}} = \pi/(2\sqrt{\Omega_A^2 + \Omega_B^2})$, the basis states at \mathbf{q}_N , which are $|\uparrow\rangle = |1\rangle$ and $|\downarrow\rangle = |3\rangle$, are mapped to $|\uparrow(\mathbf{q}_0)\rangle$ and $|\downarrow(\mathbf{q}_0)\rangle$ at $\phi_A = \phi_B = 0$, respectively. For $t_{\text{map}} = 3\pi/(2\sqrt{\Omega_A^2 + \Omega_B^2})$, the basis states at \mathbf{q} along \mathcal{C} , which are $|\uparrow(\mathbf{q})\rangle$ and $|\downarrow(\mathbf{q})\rangle$, are mapped back to $|\uparrow\rangle$ and $|\downarrow\rangle$, respectively. The former pulse operation ($\hat{U}_{\text{trans}}(t_{\text{prep}}, \mathbf{q}_0) = \hat{U}_{\text{prep}}$) is applied for preparing the eigenstates at \mathbf{q}_0 before the phase ramp, whereas the latter ($\hat{U}_{\text{trans}}(t_{\text{map}}, \mathbf{q}) = \hat{U}_{\text{map}}$) is applied after the phase ramp along the loop \mathcal{C} to read out the state.

The basis states for the degenerate subspace

We take the following eigenstates for the basis of the ground DS at \mathbf{q} for the region in the parameter space we have experimentally explored ($\delta = 0, \phi_B = 0, \phi_A \in [0, 2\pi], \theta_2 \in [0, \pi/2]$),

$$\begin{aligned} |\uparrow_{-}(\mathbf{q})\rangle &= (|1\rangle - e^{-i\phi_A} \cos \theta_2 |2\rangle + \sin \theta_2 |4\rangle) / \sqrt{2} \\ |\downarrow_{-}(\mathbf{q})\rangle &= (-\sin \theta_2 |2\rangle + |3\rangle - e^{i\phi_A} \cos \theta_2 |4\rangle) / \sqrt{2} \end{aligned} \quad (\text{S3})$$

Using the basis states, the pure state within the DS at \mathbf{q} is described by

$$|\Psi(\mathbf{q})\rangle = c_{\uparrow} |\uparrow_{-}(\mathbf{q})\rangle + c_{\downarrow} |\downarrow_{-}(\mathbf{q})\rangle, \quad (\text{S4})$$

which can be represented by a two-component spinor $\Psi = (c_{\uparrow}, c_{\downarrow})^T$, where $|c_{\uparrow}|^2 + |c_{\downarrow}|^2 = 1$ is met.

Each eigenstate can be prepared by applying the cyclic coupling pulse as described above to one of the bare spin states.

$$\begin{aligned} |\uparrow_{-}(\mathbf{q})\rangle &= \hat{U}_{\text{trans}}(t_{\text{prep}}, \mathbf{q}) |\uparrow\rangle, \\ |\downarrow_{-}(\mathbf{q})\rangle &= \hat{U}_{\text{trans}}(t_{\text{prep}}, \mathbf{q}) |\downarrow\rangle, \end{aligned} \quad (\text{S5})$$

where $|\uparrow\rangle = |1\rangle$ and $|\downarrow\rangle = |3\rangle$ is the basis state of the ground DS at \mathbf{q}_N . Therefore, the four initial eigenstates ($|A\rangle, |B\rangle, |C\rangle$ and $|D\rangle$) at \mathbf{q}_0 can be prepared by applying the pulse for the duration t_{prep} with the parameter vector \mathbf{q}_0 to the states $|\uparrow\rangle, |\downarrow\rangle, (|\uparrow\rangle + |\downarrow\rangle) / \sqrt{2}$, and $(|\uparrow\rangle + i|\downarrow\rangle) / \sqrt{2}$, respectively. For the state mapping, the basis states of the DS at \mathbf{q} can be mapped to the bare spin states.

$$\begin{aligned} |\uparrow\rangle &= -\hat{U}_{\text{trans}}(t_{\text{map}}, \mathbf{q}) |\uparrow_{-}(\mathbf{q})\rangle, \\ |\downarrow\rangle &= -\hat{U}_{\text{trans}}(t_{\text{map}}, \mathbf{q}) |\downarrow_{-}(\mathbf{q})\rangle, \end{aligned} \quad (\text{S6})$$

Quantum state tomography

After the state acquired the W.-Z phase, we measured the final state within the DS by evaluating the Bloch vector ($\langle \hat{\sigma}_x(\mathbf{q}) \rangle, \langle \hat{\sigma}_y(\mathbf{q}) \rangle, \langle \hat{\sigma}_z(\mathbf{q}) \rangle$). Here the Pauli operators are defined from the basis states of the DS at \mathbf{q} .

Using the state mapping procedure described above, the target Bloch vector is obtained by performing state tomography for the superposition states in the microwave clock transition ($|1, 0\rangle \leftrightarrow |2, 0\rangle$). The z-component was obtained from the population imbalance $(N_{\uparrow} - N_{\downarrow}) / (N_{\uparrow} + N_{\downarrow})$. The x or y-component was obtained by rotating the Bloch vector with a $\pi/2$ -pulse with an appropriate microwave phase before measuring the population imbalance.

Quantum process tomography using maximum likelihood estimation

In order to find physical process matrix χ that represents the W.-Z. phase from our measurement, we adopted maximum likelihood estimation in the quantum process tomography. For the process matrix to be physical, we define χ as

$$\chi = T^{\dagger} T / \text{tr}(T^{\dagger} T), \quad (\text{S7})$$

where T is the lower triangular matrix of the form

$$T = \begin{bmatrix} t_1 & 0 & 0 & 0 \\ t_5 + it_6 & t_2 & 0 & 0 \\ t_{11} + it_{12} & t_7 + it_8 & t_3 & 0 \\ t_{15} + it_{16} & t_{13} + it_{14} & t_9 + it_{10} & t_4 \end{bmatrix} \quad (\text{S8})$$

where $t_i, (i = 1, \dots, 16)$ is real. We define a minimizing function $f(\mathbf{t})$ as

$$f(\mathbf{t}) = \sum_j \left[\hat{\rho}_{\text{fin},j} - \left\{ \sum_{m,n} \hat{E}_m \hat{\rho}_{\text{ini}} \hat{E}_n^{\dagger} \left(\frac{T^{\dagger} T}{\text{tr}(T^{\dagger} T)} \right)_{mn} \right\}_j \right]^2, \quad (\text{S9})$$

where $\mathbf{t} = (t_1, t_2, \dots, t_{16})$, $j \in \{A, B, C, D\}$ distinguish the four initial states in the W.-Z. phase measurements, $\hat{\rho}_{\text{ini}} = |j\rangle\langle j|$, and $\hat{\rho}_{\text{fin}}$ is the density operator for the state after it traced out the (open or closed) loop \mathcal{C} . An average of measurements was used for each $\hat{\rho}_{\text{fin},j}$. We numerically minimize $f(\mathbf{t})$ for the parameter vector \mathbf{t} to obtain optimum T and the process matrix χ .

Synthetic non-Abelian SU(2) gauge field and Wilson loop

Consider a quantum system with a Hamiltonian $\hat{H}(\mathbf{q})$ that depends continuously on the position vector $\mathbf{q} = (q_1, q_2, \dots)$. The system is described by eigenstates and eigenenergies

$$\hat{H}(\mathbf{q})|\Psi_{n\alpha}(\mathbf{q})\rangle = E_n(\mathbf{q})|\Psi_{n\alpha}(\mathbf{q})\rangle, \quad (\text{S10})$$

where $|\Psi_{n\alpha}(\mathbf{q})\rangle$ ($\alpha = 1, 2, \dots, N_\alpha$) is N_α -fold degenerate eigenstate with energy E_n forming an N_α -fold degenerate subspace. For quantum states in a single energy level E_n , a gauge potential called the Berry connection

$$\mathcal{A}_{q_m}^{\alpha\beta}(\mathbf{q}) = i\langle\Psi_\alpha(\mathbf{q})|\partial/\partial q_m|\Psi_\beta(\mathbf{q})\rangle, \quad (\text{S11})$$

is encoded in the systemsEigenstates, where $\mathcal{A}_{q_m}^{\alpha\beta}$ is the m -th component of the vector gauge field \mathcal{A} represented as N_α -by- N_α matrix. Here, we omitted n in the l.h.s. for simplicity, and the matrix indices take $\alpha, \beta \in \{1, 2, \dots, N_\alpha\}$. The gauge field (Berry connection) is non-Abelian when two components of the gauge field do not commute with each other.

Now, we consider the gauge field for the Hamiltonian in Eq. (2). We focus on the parameters relevant to the experiment ($\Omega_A = \Omega \cos \theta_2$, $\Omega_B = \sin \theta_2$, $\delta = 0$, and $\phi_B = 0$). The non-Abelian SU(2) Berry connection for the two-fold degenerate ground states is

$$\begin{aligned} \mathcal{A}_{\phi_A}(\mathbf{q}) &= \frac{1}{2} \begin{pmatrix} \cos^2 \theta_2 & e^{i\phi_A} \sin \theta_2 \cos \theta_2 \\ e^{-i\phi_A} \sin \theta_2 \cos \theta_2 & -\cos^2 \theta_2 \end{pmatrix} \\ &= (\cos \phi_A \sin \theta_2 \cos \theta_2 \sigma_x - \sin \phi_A \sin \theta_2 \cos \theta_2 \sigma_y + \cos^2 \theta_2 \sigma_z)/2. \end{aligned} \quad (\text{S12})$$

From the definition in Eq. (1), we obtain W.-Z. phases factors and Wilson loops for the paths \mathcal{C}_\pm ,

$$U_{\mathcal{C}_\pm} = \begin{pmatrix} -\cos(\pi \sin \theta_2) \pm i \sin \theta_2 \sin(\pi \sin \theta_2) & \mp i \cos \theta_2 \sin(\pi \sin \theta_2) \\ \mp i \cos \theta_2 \sin(\pi \sin \theta_2) & -\cos(\pi \sin \theta_2) \mp i \sin \theta_2 \sin(\pi \sin \theta_2) \end{pmatrix}. \quad (\text{S13})$$

$$W_{\mathcal{C}_\pm} = -2 \cos(\pi \sin \theta_2). \quad (\text{S14})$$

The dependence on the ramp direction for the W.-Z. phase factors ($\hat{U}_{\mathcal{C}_+} = \hat{U}_{\mathcal{C}_-}^\dagger$), and the Wilson loops ($W_{\mathcal{C}_+} = W_{\mathcal{C}_-}^*$) can be clearly seen. Both the W.-Z. phases factor and the Wilson loop do not depend on Ω , thus they are robust against fluctuation in the coupling strength. By varying the rf phase ϕ_A , the SU(2) Wilson loop covers the full range ($-2 \leq W_{\mathcal{C}} \leq 2$), realizing various non-Abelian SU(2) holonomic controls.

Wilson line for an open path

In the following we give an argument on non-cyclic W.-Z. phase and Wilson line for an open path. The definition for non-cyclic W.-Z. phase and Wilson line are essentially the same as the cyclic case, except the integral is taken over for an open path \mathcal{C} .

$$W_{\mathcal{C}} = \text{tr}(\hat{U}_{\mathcal{C}}) = \text{tr} \left[\mathcal{P} \exp \left(i \int_{\mathcal{C}} \hat{\mathcal{A}}_{\mathbf{q}} \cdot d\mathbf{q} \right) \right], \quad (\text{S15})$$

where $\hat{\mathcal{A}}$ is non-Abelian Berry connection.

Consider a spinor state vector $|\Psi\rangle$ representing the state within the degenerate subspace (DS). Under local gauge transformation, the wavefunction transform as

$$|\Psi\rangle \rightarrow \hat{V}(\mathbf{q})|\Psi\rangle, \quad (\text{S16})$$

where $\hat{V}(\mathbf{q})$ is a position-dependent unitary operator. This can be regarded as a change in the basis states for the DS. Accordingly, the non-cyclic W.-Z. phase factor transforms as

$$\hat{U}_{\mathcal{C}} \rightarrow \hat{V}(\mathbf{q}_f) \hat{U}_{\mathcal{C}} \hat{V}^\dagger(\mathbf{q}_0), \quad (\text{S17})$$

where \mathbf{q}_0 and \mathbf{q}_f are the start point and end point of the open path \mathcal{C} , respectively. Manifestly, the r.h.s depends on the unitary operators, $\hat{V}(\mathbf{q}_0)$ and $\hat{V}(\mathbf{q}_f)$. When the trace is closed ($\mathbf{q}_0 = \mathbf{q}_f$), the Wilson line is equivalent to the Wilson loop and is gauge-independent.

For our experimental parameters for Wilson line measurement in Fig. 5 ($\delta = 0$, $\phi_B = 0$ and $\theta_2 = \pi/4$), the non-cyclic non-Abelian W.-Z phase and Wilson lines along a segment are

$$U_{\mathcal{C}} = \begin{pmatrix} e^{i\phi/2} \left[\cos\left(\frac{\phi}{2\sqrt{2}}\right) - \frac{i}{\sqrt{2}} \sin\left(\frac{\phi}{2\sqrt{2}}\right) \right] & ie^{i\phi/2} \sin\left(\frac{\phi}{2\sqrt{2}}\right) / \sqrt{2} \\ ie^{-i\phi/2} \sin\left(\frac{\phi}{2\sqrt{2}}\right) / \sqrt{2} & e^{-i\phi/2} \left[\cos\left(\frac{\phi}{2\sqrt{2}}\right) + \frac{i}{\sqrt{2}} \sin\left(\frac{\phi}{2\sqrt{2}}\right) \right] \end{pmatrix}, \quad (\text{S18})$$

$$W_{\mathcal{C}} = \sqrt{2} \sin\left(\frac{\phi}{2}\right) \sin\left(\frac{\phi}{2\sqrt{2}}\right) + 2 \cos\left(\frac{\phi}{2}\right) \cos\left(\frac{\phi}{2\sqrt{2}}\right). \quad (\text{S19})$$

Here we took the basis in Eq. (S3) for the matrix representation.

Non-adiabatic effect due to finite ramp time

Although we have focused on evolution within the ground-state manifold, a small fraction of atoms can be populated to the excited state manifold due to the finite ramp time. We experimentally confirmed this by measuring the fraction of atoms in the excited state manifold. After the state mapping, we evaluated the fraction $N_e/(N_e + N_g)$, where $N_e = N_{|2\rangle} + N_{|4\rangle}$ is the atom number in the excited state manifold, $N_g = N_{|1\rangle} + N_{|3\rangle}$ is the atom number in the ground state manifold, and $N_{|i\rangle}$ is the atom number in the bare spin state $|i\rangle$, ($i = 1, 2, 3, 4$). The observed fraction of atoms, which depends on the initial state is negligibly small, and consistent with the numerical simulation (See Fig. S1a). Longer ramp time led to a smaller fraction in the excited state manifold as confirmed by the numerical simulation [Fig. S1qb]. Experimentally, the fidelity of our holonomic control is expected to be degraded for longer ramp time due to the small but finite energy gap opening in the nearly-degenerate levels, which we assume to be about 1% of the energy gap of the system.

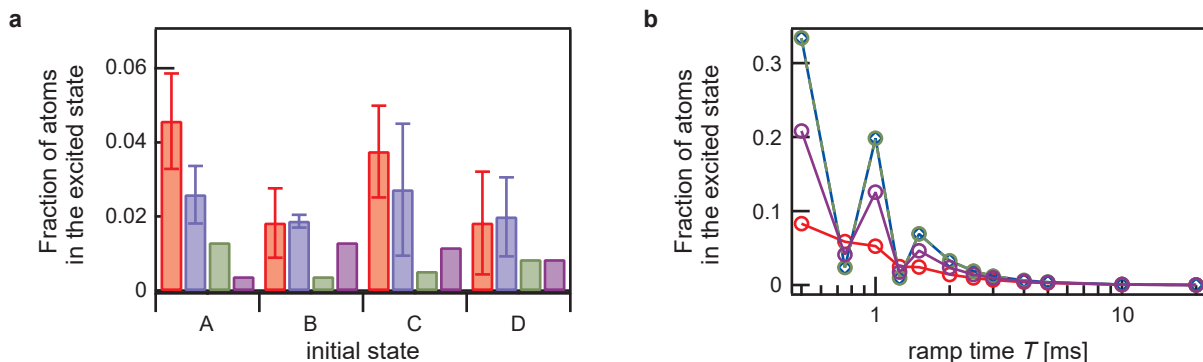


FIG. S1. Excited state population after the W.-Z. phase acquisition. (a) Experimentally and numerically obtained excited state population at $T = 2$ ms for $\theta_2 = 11\pi/36$. Experimental data for the paths \mathcal{C}_+ (red bar) and \mathcal{C}_- (blue bar) compared with numerical simulation for the paths \mathcal{C}_+ (green bar) and \mathcal{C}_- (purple bar). The error bars show the standard deviation of the data. (b) Fraction of atoms in the excited state manifold after state acquired W.-Z. phase along \mathcal{C}_- numerically simulated for the four initial states at $\theta_2 = \pi/4$. The four states are |A> (red), |B> (blue), |C> (green), and |D> (purple). Due to finite ramp time T for tracing out the loop, the non-adiabatic effect is non-negligible when the ramp rate becomes comparable to the scale of the energy gap ($\Delta E = h \times 2$ kHz).

Surprisingly, the fidelity in the W.-Z. phase measurement within the DS is robust against small non-adiabatic effect. Fig. S2 shows the numerically obtained fidelity of the W.-Z. phase by varying the ramp time. For our experimental parameters with $\theta_2 = \pi/4$, the fidelity reaches 0.998% at $T=2$ ms.

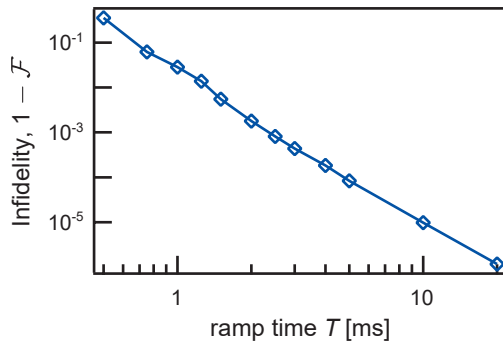


FIG. S2. Infidelity of the non-Abelian W.-Z. phase ($1 - \mathcal{F}$) due to finite ramp time T . The non-Abelian W.-Z. phase factor is numerically evaluated by solving time-dependent Schrödinger equation for our experimental condition for the path \mathcal{C}_- with $\theta_2 = \pi/4$ and analyzed by following the same procedure used in the experiment to numerically obtain the process matrix.

Measurement of the energy gap

The energy gap can be clearly measured by inducing coherent Rabi-like oscillations between the eigenstates. Figure S3 shows that the time evolution of the population imbalance $(N_e - N_g)/(N_e + N_g)$ after abruptly turning on the cyclic coupling described by the Hamiltonian in Eq. (2). Since the system has only two eigenenergies, the state oscillates between the ground and excited eigenstates at the frequency determined by the energy gap.

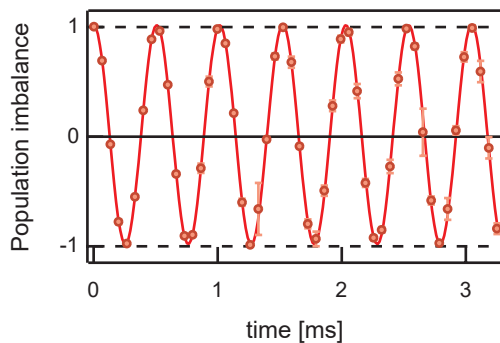


FIG. S3. Rabi-like oscillation between the two eigenstates. The population imbalance $(N_g - N_e)/(N_g + N_e)$ was measured after the cyclic coupling for $\theta_2 = \pi/4$ was abruptly turned on with the BEC in state $|2\rangle$. The observed oscillation frequency of 2.0 kHz determines the energy gap of our system. The error bars show the standard deviation of the data.